2020 IMEKO TC-19 International Workshop on
Metrology for the Sea
Naples, Italy, October 5-7, 2020

Design and verification of a “Fixed-Point” spar buoy scale model for a “Lab on Sea” unit

D. Alizzio[1], M. Bonfanti[2], N. Donato[1], C. Faraci[1], G. Grasso[2], F. Lo Savio[3], R. Montanini[1], A. Quattrocchi[1]

[1] Dept. of Engineering, University of Messina, Cont.da Di Dio, 98166 Messina, Italy.
[2] Dept. of Electric., Electron., Infor. Eng., Univ. of Catania, Via S. Sofia, 54, 95100 Catania, Italy.
[3] Dept. of Civil Eng. and Arch., University of Catania, Via S. Sofia, 54, 95100 Catania, Italy.
Corresponding Author e-mail: roberto.montanini@unime.it

***Abstract* – The present work is a part of a larger project relative to design of an instrumented spar buoy within the multi-purpose “Lab on Sea” unit equipped with an energy harvesting system for use in marine applications. Such a system will be based on deformable bands integral to the unit to convert the wave motion energy into electricity through piezo patch transducers.**
In this paper, a “fixed-point” spar buoy scale model suitable for tests in a controlled ripples-type wave motion channel was designed, built and tested. The purpose of this model is to verify that it remains fixed maximizing, then, the displacement of the bands under wave motion.
To evaluate its response, the buoy scale model was equipped with a measuring device consisting of a MEMS accelerometer and a gyroscope. Results of acquisitions from on-board sensors revealed a very low susceptibility of the buoy scale model to the wave motion imposed.

I. INTRODUCTION

Nowadays monitoring of the marine habitat is a topic of great relevance [1]. These environments are particularly susceptible to human activity, in terms of industrial and civil development. Therefore, acquiring information on sufficiently large spatial and temporal literature scales is essential to guarantee effective monitoring in order to produce solutions aimed at reducing the anthropogenic impact on ecosystems. These include monitoring the concentration of pollutants in both natural and artificial reservoirs and near sewage, the detection of microplastics and their concentration in lagoon or open sea waters [2, 3]. In addition, there are also multiple civil protection purposes, including the possibility of detecting anomalous waves or tsunamis that can occur on the coasts [4]. The scientific literature is rich of solutions involving the use of floating devices equipped with a wide range of sensors for environmental monitoring and adequate telecommunication interfaces. The most sophisticated devices employ energy recovery systems for self-maintenance (e.g. energy harvesting) so that they can be used off-shore [5]. Observation platforms include various types: on site, equipped with remote instrumentation, operating on the surface (on board an oceanographic ship [6], surface buoys [7, 8], floating buoys [9, 10], buoys towed by boats [11]), active on the seabed (autonomous underwater vehicles AUV [12], remote control vehicles ROV [13], networks of underwater buoys [14]) and with satellite monitoring [15]. The choice of the type of buoy and the equipment to be adopted is mainly determined by the characteristics of the environment to be investigated (depth of the waters, peculiarities of the waves, etc.) and the required space-time coverage [16].

In this context, the subject of this paper concerns some preparatory operations for the future design of a multi-purpose "Lab on Sea" unit able to perform energy storage automatically from waves and equipped with a communication network able of connecting to any IT infrastructure.

The idea of building a unit equipped with power systems from renewable sources to minimize the implementation and maintenance costs of the entire data collection system and to ensure energy autonomy was deemed convenient. The ultimate purpose of this investigation consists in designing additional elements of the unit able to perform energy harvesting. Thus, the target will be to develop a system with deformable and wave-sensitive bands to convert the mechanical deformation energy into electricity through piezo patch transducers. Since piezoelectric elements are more performing at high frequencies, these bands will be sensitive to ripples-type waves. In order to amplify the input of the transducers, it will be necessary to maximize the deformation by constraining the unit to remain fixed with respect to the wave motion. Hereafter such a condition is named “fixed point” (as in Fig. 1).

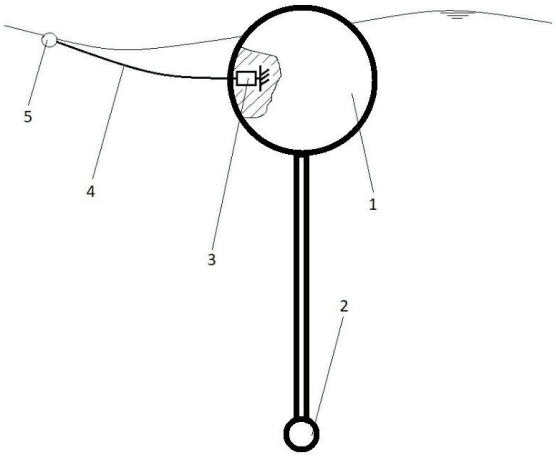

Fig. 1. Scheme of the energy conversion apparatus for the Lab on sea unit: 1. spar buoy; 2. ballast; 3. piezo patch transducer; 4. deformable band; 5. external float.

Consequentially, evaluating if the amount of the energy available through the sea wave motion is enough to recharge the on-board power supplies should be made. In this paper the dynamic behaviour of a spar buoy scale model undergone to a known wave motion was investigated in order to verify that the "fixed point condition" was satisfied.

The scale model can be assimilated to a 2 DOF mass-spring-damper system and, therefore, it was sized to make both vertical and angular oscillations negligible [17].

As known, a mass-spring-damper system of mass m, stiffness k and viscosity β, placed on a vibrating body (such as a fluid subject to wave motion) under an oscillation $x = X_0 \sin(\omega t)$ with respect to a fixed reference system, is characterized by the following equation of motion [18]:

$$m\ddot{y} + \beta\dot{y} + ky = m\omega^2 X_0 \sin(\omega t) \tag{1}$$

The ratio between the amplitudes of the dynamical response (Y_0) and the forced excitation (X_0) depends on the pulsation of the excitation (ω), the pulsation of the system ($\omega_0 = (k/m)^{1/2}$), the viscosity (β) and the critical value viscosity ($\beta_{cr} = 2(k \cdot m)^{1/2}$):

$$\frac{Y_0}{X_0} = \frac{\lambda^2}{\sqrt{(1-\lambda^2)^2 + 4\tau^2\lambda^2}} \tag{2}$$

and the phase angle (φ) between the dynamical response and the forced excitation is given by:

$$\varphi = \tan^{-1}\left(\frac{-2\tau\lambda}{1-\lambda^2}\right) \tag{3}$$

where $\lambda = \omega/\omega_0$ and $\tau = \beta/\beta_{cr}$. The aim is creating a system with high values of λ, so that the ratio between the amplitudes tends to 1 and the phase angle (φ) to π regardless of τ. This leads to a response having an amplitude equal to that of the excitation but in the counter-phase (i.e. the buoy is integral with the wave motion but in the opposite direction). Furthermore, since for high values of λ the effect of viscosity is almost negligible, the verification of angular oscillations can be traced back to the study of the harmonic motion of a simple pendulum having length L and natural frequency $\omega_n = (g/L)^{1/2}$.

II. MATERIALS AND METHODS

The spar buoy scale model designed in the present paper consists of a spherical buoy with a central through hole where a rigid rod is inserted. The rod has the dual purpose of supporting a stabilizing counterweight (ballast) in its immersed part, and accommodating the sensors and mechanical connection for the dynamic measuring instrumentation on the top (Fig. 2).

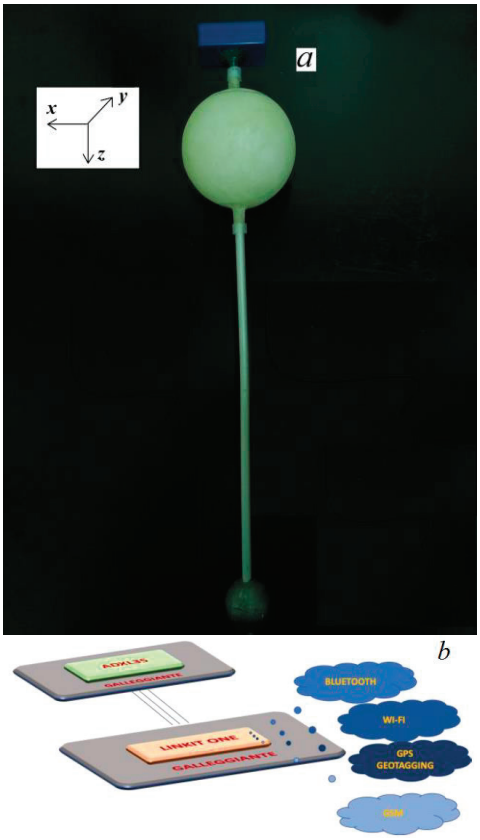

Fig. 2. (a) Spar buoy scale model; (b) block diagram of the data acquisition system.

First of all, a preliminary study on both sea and tank tests was carried out for measuring the fundamental characteristics of the wave motion (amplitude and frequency). Indeed, the knowledge of wave frequencies is fundamental to rightly design the spar buoy, above all in compliance with the required "fixed point" condition.

It was found that the trend of the measured acceleration appears to be sufficiently repeatable in both conditions. Furthermore, frequency distributions are comparable despite the different way to excitate. The most representative frequency values found for ripples-type waves ranged from 1 to 3 Hz. Fig. 3 shows the comparison between the vertical accelerations measured at sea (near the shore in the coastal area) and under controlled conditions (artificial canal), and the comparison between their respective signals in frequency domain (DFT).

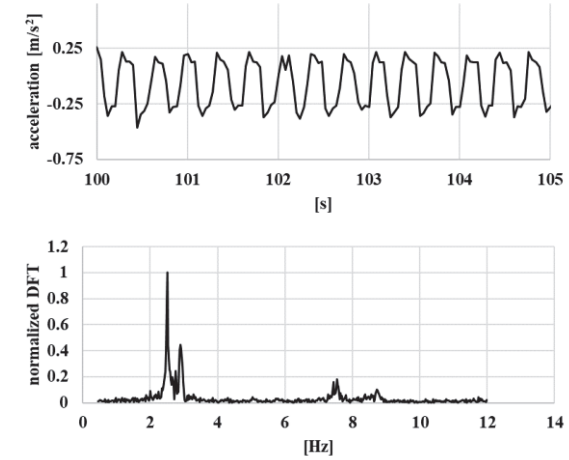

(a)

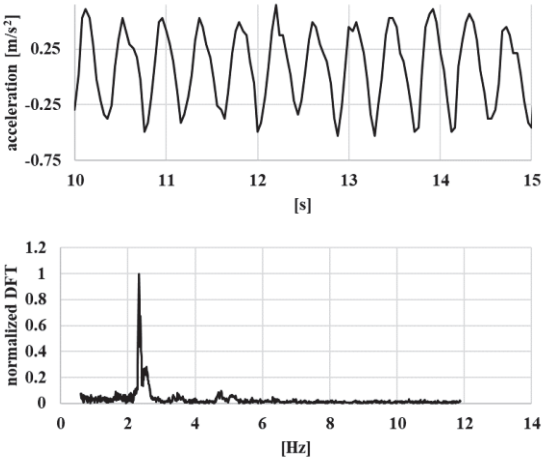

(b)

Fig. 3. Comparison between acceleration and normalized DFT (a) at sea and (b) in artificial canal

d	*S*	*B*	H_e	*M*	*L*	λ_{vert}	λ_{ang}
[mm]	*[mm]*	*[N]*	*[mm]*	*[kg]*	*[mm]*		
600	*500*	*1052.5*	*100*	*57.5*	*2000*	*10.62*	*5.67*

Table 1. Summary on the buoy unit sizing.

From a preliminary analysis of the comparison between the measurements at sea and within an artificial canal, it was analytically found that the geometric dimensions allowing the unit, subjected to the forced excitations, to satisfy the “fixed point” condition are shown in Tab. 1. However, in order to experimentally verify that the Lab on sea unity will be capable of satisfying the required "fixed point" condition, a scale model was created because it is best suited to tank tests. Indeed, the water measurement system available consisted of a channel for the production of an established wave motion, having a wet section of 600x600 mm and a length of 10 m. It was equipped with an air system for the generation of ripples-type waves and a measuring device for real-time reading of the wave height and frequency.

Tab. 2 shows the geometric and mechanical scale data for the buoy model and its counterweight. Having imposed a value of 100 mm for the diameter *d* of the buoy model (linear scale factor of 1/6), the choice of values useful for sinking *S* was made so as to fall within the linear section of the relative "buoyancy-sinking" curve. In particular, the value of 86 mm was chosen for *S*, which corresponds to a buoyancy *B* of nearly 3.98 N, and the value of 14 mm was set for the emerged height of the spherical cap H_e. The ballast, also spherical in shape and made of lead (density of 11.34 kg/dm^3), provided a counterweight of mass *M* equal to 0.45 kg and was placed from the buoy centre at a barycentric distance *L*= 370 mm.

Considering 2.5 Hz as the most representative average value found for the oscillation frequency, the sizing of the buoy model provided sufficiently high values of λ (see section I) both as regards vertical oscillations (λ_{vert} = 12.73) than the angular ones (λ_{ang} = 14.69).

d	*S*	*B*	H_e	*M*	*L*	λ_{vert}	λ_{ang}
[mm]	*[mm]*	*[N]*	*[mm]*	*[kg]*	*[mm]*		
100	*86*	*3.98*	*14*	*0.45*	*370*	*12.73*	*14.69*

Table 2. Summary on the buoy model sizing.

The model of the buoy built consists of a polystyrene sphere coated by deposition of polyester thermosetting epoxy powder.

The counterweight was made of lead by means of a casting process on a special plaster mould. The rigid rod for connecting the counterweight to the buoy consists of a

cylindrical aluminium tubular with external diameter of 10 mm and thickness of 1 mm. On the top of the rod, a cylindrical seat accommodating a displacement sensor (iNEMO inertial module included in ST SensorTile.box) was obtained. This sensor consisted of a triaxial gyroscope and a triaxial accelerometer. It was internally power supplied and it allowed an easy reading of the measured quantities via Bluetooth communication and data logging on internal SD card. Measurement range was selected between -500 deg/s and +500 deg/s for gyroscope and -39.24 m/s^2 and +39.24 m/s^2 for accelerometer. Data sampling was performed at 104.0 Hz both for accelerometer and gyroscope signals, corresponding to a bandwidth cut-off frequency of 33.0 Hz according to sensors signal chain characteristics in low energy mode. In this configuration, gyroscope has RMS rate noise value of 0.075 deg/s, while accelerometer has RMS rate noise value of 0.01962 m/s^2. The sensitivity tolerance is ±1% on the measurement value both for the accelerometer and the gyroscope. The temperature affects the accelerometer measurement in order of ±0.01% and the gyroscope measurement in order of ±0.007%.

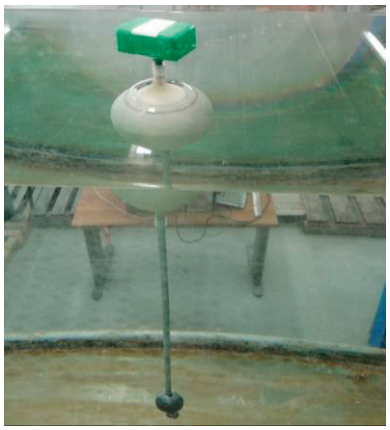

Fig. 4. Spar buoy scale model test

A dynamic buoyancy test of the scale model in the above-mentioned controlled water channel was performed at room temperature of 25 °C (Fig. 4). The ripples-type waves were monitored via image acquisition and post-processed. For the acquisition, a camera Basler acA1300-30 gm GigE with a CCD sensor (Sony ICX445, resolution of 1296 px. 966 px), a 35 mm lens (C23-3520-2 M F2.0) was used. A motion reconstruction of the ripples-type waves was computed through NI Image Acquisition module on LabView environment. As shown in Fig. 5, the average value found for the imposed oscillation frequency was of 2.63 Hz, in line with the most representative frequency values of ripples-type waves. Acquisitions from both on-board accelerometer and gyroscope was performed at 104 Hz. The ST SensorTile.box mounted on the scale buoy returned values confirming the accomplishment of the required "fixed point condition".

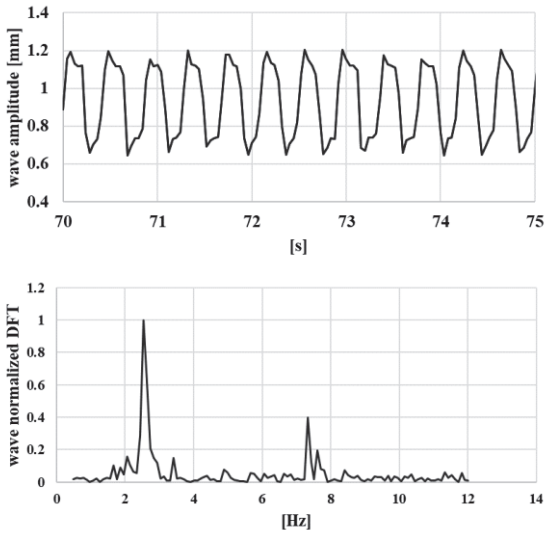

Fig. 5. Wave amplitude and normalized DFT in controlled water channel.

As expected, the Z-signal from the accelerometer of ST remained constant for the whole test and equal to nearly -9.73 m/s^2 (Fig. 6 and Tab. 3), and it means that the scale buoy remained integral to the vertical wave motion. The 3-axis gyroscope also did not detect appreciable variations in angular oscillations returning mean values about 0.40 deg/s around X-axis and -0.63 deg/s around Y-axis.

	max	*min*	*mean value*	*st. deviation*
	[m/s^2]	*[m/s^2]*	*[m/s^2]*	*[m/s^2]*
X axis	*0,28449*	*-0,13734*	*0,07633*	*0,065729*
Y axis	*0,04905*	*-0,53955*	*-0,2377*	*0,075556*
Z axis	*-9,59418*	*-9,83943*	*-9,73372*	*0,029311*

Table 3. Data from 3-axial accelerometer in iNEMO inertial module

	max	*min*	*mean value*	*st. deviation*
	[deg/s]	*[deg/s]*	*[deg/s]*	*[deg/s]*
X axis	*1,9*	*-1,6*	*0,401346*	*0,569683*
Y axis	*0,9*	*-1,9*	*-0,62611*	*0,472373*
Z axis	*9,5*	*-9*	*-0,3975*	*3,103408*

Table 4. Data from 3-axial gyroscope in iNEMO inertial module

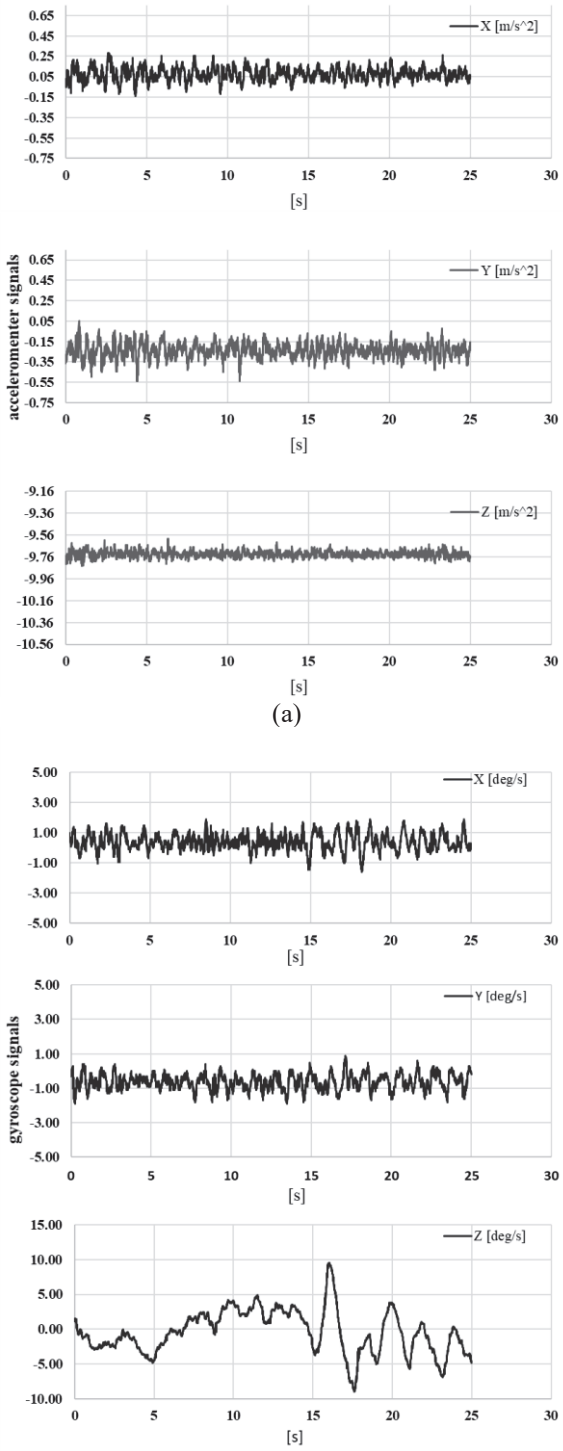

Fig. 6. Signals from (a) accelerometer and (b) gyroscope in iNEMO inertial module.

III. CONCLUSIONS

As expected, the low values found for both vertical and angular oscillations confirm compliance with the "fixed point" condition required. In particular, the average value of vertical oscillations along the Z-axis direction equals to -9.73 m/s^2, meaning that the scale buoy is invariant respect to the vertical wave motion. Moreover, the average values of both angular oscillations around the X-axis and Y-axis are equal to 0.40 deg/s and -0.63 deg/s respectively, as a confirmation of maintaining horizontal position with respect the free surface of the water.

REFERENCES

[1] C. Albaladejo, F. Soto, R. Torres, P. Sánchez, J.A. López, A Low-Cost Sensor Buoy System for Monitoring Shallow Marine Environments, Sensors 2012, 12, 9613-9634; doi:10.3390/s120709613.

[2] G.F. Schirinzi, M. Llorca, R. Serò, E. Moyano, D. Barcelò, E. Abad, M. Farrè, Trace analysis of polystyrene microplastics in natural water, Chemosphere 2019, 236, doi.org/10.1016/j.chemosphere.2019.07.052.

[3] S. Savoca, G. Capillo, M. Mancuso, C. Faggio, G. Panarello, R. Crupi, M. Bonsignore, L. D'Urso, G. Compagnini, F. Neri, E. Fazio, T. Romeo, T. Bottari, N. Spanò, Detection of artificial cellulose microfibers in Boops boops from the northern coasts of Sicily (Central Mediterranean), Science of the Total Enviroment 2019, Vol. 691, 455-465.

[4] X. Roset, E. Trullos, C. Artero-Delgado, J. Prat, J. Del Rio, I. Massana, M. Carbonell, G. Barco de la Torre, D. Mihai Toma, Real-Time Seismic Data from the Bottom Sea, Sensors 2018, 18, doi: 10.3390/s18041132.

[5] Dong Yeong Kima, Hyun Soo Kima, Dae Sol Konga, Moonkang Choib, Hak Bum Kima, Jae-Hyoung Leec, Gonzalo Murillod, Minbaek Leeb, Sang Sub Kimc, Jong Hoon Junga, Floating buoy-based triboelectric nanogenerator for an effective vibrational energy harvesting from irregular and random water waves in wild sea, Nano Energy 45 (2018) 247-254, http://dx.doi.org/10.1016/j.nanoen.2017.12.052.

[6] C.A Balfour, M.J. Howarth, M.J. Smithson, D.S. Jones, J. Pugh, The Use of Ships of Opportunity for Irish Sea Based Oceanographic Measurements, In Proceedings of the IEEE Conference OCEANS, Vancouver, BC, Canada, 29 September–4 October 2007, 1–6.

[7] Z. Chenbing, W. Xinpeng, L. Xiyao, Z. Suoping, W. Haitao, A small buoy for flux measurement in air-sea boundary layer, In Proceedings of the ICEMI 2017, doi: 10.1109/ICEMI.2017.8265999.

[8] U.M. Cella, N. Shuley, R. Johnstone, Wireless Sensor

Networks in Coastal Marine Environments: A Study Case Outcome, In Proceedings of V International Workshop on UnderWater Networks 2019, 1-8.
[9] L. Emery, R. Smith, D. McNeal, B. Hughes, W. Swick, J. MacMahan, Autonomous Collection of River Parameters Using Drifting Buoys, In Proceedings of the IEEE Conference OCEANS, Seattle, WA, USA, 20–23 September 2010, 1–7.
[10] A. Kwok, S. Martinez, Deployment of Drifters in a Piecewise-constant Flow Environment, In Proceedings of the 49th IEEE Conference on Decision and Control (CDC), Atlanta, GA, USA, 15–17 September 2010, 6584–6589.
[11] J.K. Choi, T. Shiraishi, T. Tanaka, H. Kondo, Safe operation of an autonomous underwater towed vehicle: Towed force monitoring and control, Autom. Constr. 2011, 20, 1012–1019.
[12] I. Masmitja, G. Masmitja, J. Gonzalez, S. Shariat-Panahi, S. Gomariz, Development of a control system for an Autonomous Underwater Vehicle, In Proceedings of the 2010 IEEE/OES Autonomous Underwater Vehicles (AUV), Monterey, CA, USA, 1–3 September 2010, doi: 10.1109/AUV.2010.5779647.
[13] D.B. Duraibabu, S. Poeggel, E. Omerdic, R. Capocci, E. Lewis, T. Newe, G. Leen, D. Toal, G. Dooly, An Optical Fibre Depth (Pressure) Sensor for Remote Operated Vehicles in Underwater Applications, Sensors 2017, 17(2), 406, doi: 10.3390/s17020406.
[14] I.F. Akyildiz, D. Pompili, T. Melodia, Underwater acoustic sensor networks: Research challenges, Ad Hoc Networks 2005, 3, 257–279, doi: 10.1016/j.adhoc.2005.01.004.
[15] S. Calmant, F. Seyler, J.F. Cretaux, Monitoring Continental Surface Waters by Satellite Altimetry, Surveys in Geophysics 2009, 4-5, 247-269.
[16] D. Prandle Operational oceanography—A view ahead, Coast. Eng. 2000, 41, 353–359.
[17] M.E. McCormick, Ocean Engineering Mechanics: With Applications, Cambridge University 2010
[18] G. Diana, F. Cheli, Dinamica dei sistemi meccanici, Polipress 2010, vol. 1, 146-157.